Shuffle-induced Modulated Structure and Heating-induced Ordering in the Metastable β-Titanium Alloy, Ti-5Al-5Mo-5V-3Cr

Yufeng Zheng [a, b, *], Stoichko Antonov [c, *], Qiang Feng [c], Rajarshi Banerjee [d], Dipankar Banerjee [e] and Hamish L. Fraser [a]

[a] Center for the Accelerated Maturation of Materials and Department of Materials Science and Engineering, The Ohio State University, Columbus, OH 43212, USA.
[b] Department of Chemical and Materials Engineering, University of Nevada Reno, Reno, NV 89557, USA
[c] Beijing Advanced Innovation Center for Material Genome Engineering, State Key Laboratory for Advanced Metals and Materials, University of Science and Technology Beijing, Beijing, China
[d] Materials Research Facility and Department of Materials Science and Engineering, University of North Texas, Denton, TX 76207, USA
[e] Department of Materials Engineering, Indian Institute of Science, Bengaluru, Karnataka 560012, India

* Corresponding author: Yufeng Zheng, yufengz@unr.edu, Department of Chemical and Materials Engineering, University of Nevada Reno, 1664 N. Virginia St., Reno, NV 89557, USA; Stoichko Antonov, antonov@ustb.edu.cn, Beijing Advanced Innovation Center for Material Genome Engineering, State Key Laboratory for Advanced Metals and Materials, University of Science and Technology Beijing, Beijing, China

Abstract

A nano-scaled shuffle-induced modulated structure and heating-induced ordering have been characterized in a metastable β-titanium alloy, Ti-5Al-5Mo-5V-3Cr, and their inter-relationship was investigated through in-situ and ex-situ conventional and aberration-corrected scanning/transmission electron microscopy and atom probe tomography. The nano-scaled O' phase with a disordered orthorhombic-modulated structure formed by the $\{011\}\langle 01\bar{1}\rangle_{\beta}$ transverse phonon was characterized for the first time to be stable from room temperature to ~200°C. The O" phase with an ordered orthorhombic structure formed from the β phase during aging above the O' phase solvus temperature, where Al segregation in nano-scaled regions led to ordering of every third {011} planes.

Keywords: Titanium alloys; Modulated structure; Ordering; High resolution transmission electron microscopy; Atom probe tomography

Microstructural evolution and mechanical performance of metastable β-titanium alloys are closely related to the stability of the β phase [1, 2] which can result in various nano-scaled instabilities [3-12], and so can therefore be manipulated using different thermomechanical processing routines [13, 14]. For example, in the ultra-high strength metastable β-titanium alloys, nano-scaled metastable ω phase with an hexagonal structure can act as potential nucleation sites for subsequent α phase precipitation [15, 16]. This can improve the strength of metastable β-

titanium alloys while maintaining considerable ductility [17, 18]. Much attention has been focused on the various deformation mechanisms involved in metastable β-titanium alloys, e.g., gum metal, indicating that, depending on the β phase stability, dislocation slip, deformation twinning, and deformation induced martensitic transformation can occur [19-25]. The origin of these deformation mechanisms, such as that of {332}<113> type deformation twining [7, 21, 26] as well as a deformation induced martensitic transformation (orthorhombic structure α" phase) [9, 27], is still in debate. One critical factor involved in these proposed mechanisms is believed to be the nano-scaled modulated domains [6, 7, 27, 28], where the orthorhombic structure of these modulated domains accelerates the formation of {332}<113> twining due to the more energetically favorable magnitude of twinning shear and shuffle involved [7]. Therefore, in order to achieve a better understanding of novel phase transformation mechanisms as well as deformation mechanisms in metastable β-titanium alloys, a systematic investigation of various types of nano-scaled structural and compositional instabilities and their responses to different parameters, such as chemical composition, temperature and external stress, is required.

Recently, several different novel nano-scaled structural instabilities, besides the ω phase, that form when the concentration of solutes in the β phase exceeds a critical value, have been explored in a variety of metastable β-titanium alloys. In the eutectoid type β-titanium alloys, nano-scaled incommensurate modulated domains have been observed in a Ti-Fe alloy containing >13.8wt%Fe, in which the atoms deviate from the perfect bcc lattice sites without showing fixed long range periodicity and the disordered arrangements of atoms in these domains are found not related to the shuffle mechanism involved in the formation of ω phase [29]. Similar nano-scaled incommensurate modulated domains have also been observed in Ti-Mn, Ti-Cr and Ti-Mo-Fe alloys [30-32]. In isomorphous β-titanium alloys, nano-scaled O' phase, formed by the $\{110\}\langle 1\bar{1}0\rangle$ transverse phonon (atom shuffle of every other {110} plane along a $\langle 1\bar{1}0\rangle$ direction), that breaks the bcc symmetry into orthorhombic symmetry, was observed in Ti-Mo [12, 33], Ti-Nb-Zr [5, 11] and Ti-Mo-Al alloys [34]. Phases with similar structures (based on TEM diffraction patterns) have also been observed in other multifunctional β-titanium alloys, such as Ti-Nb-Ta-Zr-O alloy [35] and oxygen-doped Ti-Nb based alloys [6, 27]. It was also noticed that in Ti-Nb-O alloy, the unique superelasticity and the temperature dependent shape memory effect are explained by the reversible transformation between the nano-scaled modulated domains and long-range α" martensite, where the oxygen diffusion at the elevated temperature reduces the local barrier to long-range α" martensite formation, and then such α" martensite can form by heating [27]. However, such heating-induced martensite has not been widely observed in aged β-titanium alloys. In contrast, in the alloy Ti-5Al-5Mo-5V-3Cr (Ti-5553) when aged, a novel ordered orthorhombic structure O" phase was recently characterized [36]. Therefore, the stability of nano-scaled O' phase in metastable β-titanium alloys, especially its response to temperature excursions, still requires further exploration and its relationship with heating-induced long-ranged α" martensite needs to be verified.

In the current work, in-situ and ex-situ characterization techniques were employed in a heat treatment study involving Ti-5553 focusing on the following topics: (1) exploration of the modulated structure in a commercial titanium alloy; (2) investigation of the stability of such modulated structure, especially its response to thermal exposure at elevated temperatures; (3) verification of the inter-relationship between the modulated structure and the ordered structure during aging.

A description of the raw material of Ti-5553 and the equipment used have been provided previously [15]. The raw material was provided by TIMET Company and its chemical composition as determined by wet chemistry, and also atom probe tomography (APT), is provided in Table 1. Using an Electro-Thermal-Mechanical-Tester (ETMT), the alloy was solution treated at 1000°C for 30 minutes (β transus temperature ≈ 855°C), fast cooled to room temperature, then heated to 350°C and 375°C at a rate of 5°C/min, and subsequently fast cooled to room temperature. Thin foils along specific orientations were prepared for transmission electron microscopy (TEM) using a Dual Beam-Focused Ion Beam (DB-FIB) technique, a FEI Helios Nanolab 600 system, and were cleaned at low voltage using a Fischione Model 1040 Nanomill. TEM dark field images and diffraction patterns were recorded at room temperature (RT) and elevated temperatures using an FEI Tecnai G2-30 transmission electron microscope operating at an accelerating voltage of 300kV, using a Gatan model 652 heating in-situ holder. High angle annular dark field-scanning transmission electron microscopy (HAADF-STEM) images were recorded using a probe-corrected FEI Titan3™ 80-300 at 300kV. APT samples were also prepared using a DB-FIB technique, utilizing 5 kV Ga^+ ions as the final cleaning step. The APT experiments were conducted on a LEAP™ 5000XR system at a base temperature of 30K, laser pulse energy of 10 pJ, pulse repetition rate of 250 kHz and up to 2% detection rate. The data was analyzed with IVAS 3.8.2 software from Cameca Instruments Inc.

The microstructure of the as-quenched state Ti-5553 was explored using conventional and aberration-corrected S/TEM and the results are shown in Fig. 1(a-e). In the $[011]_\beta$ zone axis diffraction pattern (Fig. 1(a)), besides ω phase reflections located at 1/3 and 2/3 $\{21\bar{1}\}_\beta$, extra reflections at 1/2 $\{21\bar{1}\}_\beta$ can also be observed, demonstrated in the inset line intensity profile along the yellow color dotted-line in the figure. Such reflections belong to the orthorhombic O' phase structure [5]. In the corresponding dark field image, (Fig. 1(b)), imaged using the reflections in the yellow circle, athermal ω phase particles and O' phase particles can be observed co-existing as nano-scaled domains. In the $[100]_\beta$ zone axis diffraction pattern and its corresponding dark field image, only reflections belonging to O' phase can be observed at 1/2 $\{013\}_\beta$, supported by the inset line profile along the yellow dotted-line marked, and nano-scaled O' particles are distributed in the parent β phase. The structure of O' phase was investigated using atomic resolution HAADF-STEM imaging in the $[011]_\beta$ direction, shown in Fig. 1(e). In the highlighted O' phase domains (yellow color circle) periodic lattice modulations can be observed, indicating that the atoms on every other $(011)_\beta$ planes shuffle along the $[01\bar{1}]_\beta$ direction. The results displayed in Fig. 1(a-e) have shown for the first time unambiguous evidence of the $\{011\}\langle 01\bar{1}\rangle_\beta$ shuffle-produced modulated structure of orthorhombic symmetry together with athermal ω phase of hexagonal structure in the as-quenched state Ti-5553. Thus, in all the previous studies, shuffle-induced modulated structure (O' phase) has only been observed in gum-like titanium alloys possessing significant ductility, e.g., Ti-26Nb-2Zr (at%), Ti-18Mo (wt%) and Ti-24Nb-4Zr-8Sn (wt%) [5, 33, 34], as well as modulated domains in Ti-Nb-O alloy and Ti-23Nb-2Zr-0.7Ta-1.2O [6, 27, 28]. These alloys are located near the boundary in the $\overline{Bo}$-$\overline{Md}$ diagram where martensite is avoided [1]. However, our current results show that $\{011\}\langle 01\bar{1}\rangle_\beta$ shuffling can occur in a broader range of metastable β-titanium alloys, as long as the overall solute content exceeds a critical value as predicted using first principle calculations [12], such as in Ti-5553 which contains significant amounts of β phase stabilizers (molybdenum equivalency

≈ 18wt% [37]) designed for high strength, which in the $\overline{Bo}$-$\overline{Md}$ diagram is located in the α+ β alloys region [38].

The stability of the O' phase at elevated temperatures was investigated using an in-situ TEM heating holder. The $[100]_\beta$ zone axis diffraction patterns from the aged Ti-5553 sample were recorded from RT up to 350°C, shown in Fig. 2(a-h). O' phase reflections at 1/2 $\{013\}_\beta$ can be observed in each diffraction pattern from Fig. 2(a-e), indicating that the O' phase exists in the aged sample in a broad range of temperatures from RT to 200°C, and the intensity of O' phase reflections weakens gradually as the temperature increases. At a temperature equal to or above 250°C (e.g. 350°C shown in Fig. 2(h)), O' phase reflections cannot be identified clearly leaving only β phase reflections, revealing a transformation of O' phase to the parent β phase. This in-situ characterization using TEM and a heating stage shows that the nano-scaled shuffle-induced O' phase formed during quenching is stable in a wide temperature range, from RT to as high as 200°C, but it will revert to the β phase at a critical temperature likely via a reverse atom shuffle mechanism instead of transforming to α" phase. In the nomenclature used with the ω phase, the critical temperature is named the O' phase solvus temperature. The measured O' phase solvus temperature for Ti-5553 is between 200°C and 250°C, higher than the reported solvus temperature of modulated domains (~373K) in Ti-23Nb-1.0O [27].

To explore the evolution of the O' phase, further TEM analyses were carried out using the samples that were first continuously heated to a temperature above O' phase solvus temperature, 350°C and 375°C, and the results are compared in Fig. 3(a-f). In the sample heated to 350°C, strong ω phase reflections at 1/3 and 2/3 $\{21\bar{1}\}_\beta$ and weak O' phase reflections at 1/2 $\{21\bar{1}\}_\beta$ are observed in the $[011]_\beta$ zone axis diffraction pattern in Fig. 3(a). In the corresponding dark field image formed by selecting the reflections in the yellow color circles, only isothermal ω phase (ω_{iso}) particles were observed in Fig. 3(c). In the $[100]_\beta$ zone axis diffraction pattern, only O' phase reflections of very low intensity can be observed in Fig. 3(b), indicating the formation of O' phase in the final quenching process from 350°C to RT. In contrast, in the sample heated to 375°C, besides ω_{iso} reflections, extra reflections belonging to O" phase appear at 1/3 and 2/3 of $\{01\bar{1}\}_\beta$ in both $[011]_\beta$ and $[100]_\beta$ zone axis diffraction patterns marked in Fig. 3(d-e). In the corresponding dark field image, Fig. 3(f), selecting the reflections highlighted in Fig. 3(e), O" phase particles exhibit ellipsoidal morphology of a size similar to that of the ω_{iso} particles in Fig. 3(c). Combined with the in-situ characterization shown in Fig. 2, the current results show that O' transforms to β phase during continuous aging between 200°C and 250°C, ω_{iso} has been formed at 350°C and the O" phase forms directly from β phase at 375°C.

The structure of O" phase observed in Ti-5553 at 375°C was further analyzed using aberration-corrected S/TEM, shown in Fig. 4(a-d). In the Z-contrast HAADF-STEM image in Fig. 4(a), two different variants of ordered O" phase are observed and highlighted by the yellow and green color ellipses. Both of these variants exhibit the ordering of every third atom plane along $[011]_\beta$ and $[0\bar{1}1]_\beta$ direction, as demonstrated by the local Fast Fourier Transform (FFT) shown in Fig. 4(b-c). In a higher magnification HAADF-STEM image focusing on one O" phase particle in Fig. 4(d), periodic atom column intensity changes along $[0\bar{1}1]_\beta$ direction can be clearly observed, revealing the ordering of every three $(0\bar{1}1)_\beta$ planes. Combining the characterization results shown in Fig. 3 and 4, once the Ti-5553 is heated above the O' solvus temperature, the ordered O" phase may form from the β phase matrix in Ti-5553, rather than the heating-induced long-

range α" martensite found in the alloy Ti-23Nb-1O [27]. APT was used to further determine the chemical nature of the O" phase. Fig 4(e) shows a 3D reconstruction containing ~19 million atoms, where only Ti ions are shown, as well as an 85 at.% Ti and 6.5 at.% Al isoconcentration surfaces. Fig. 4 (f) and (g) show a representative O" and ω_{iso} phase particle, respectively, where the higher number density O" particles are slightly smaller and more round compared with the ω_{iso} particles, which are aligned along the $<111>_{\beta}$ directions. Fig. 4 (h) and (i) show 2D concentration maps for Ti and Al from a 5 nm thick cross-section slice of O" and ω_{iso}, respectively. The scale ranges were kept constant for each respective element and show that both phases are rich in Ti and depleted in Al, O" phase less so, compared with the matrix. Proximity histograms were calculated for the two particles in Fig. 4(f) and (g) and are shown in Fig. 4(j) and (k), respectively, while the average composition of each phase is given in the Table 1. In agreement with literature [15, 39, 40], the ω_{iso} phase is depleted in all solutes and very rich in Ti, Fig 4(k), and interestingly, a slight Al segregation was observed at the ω_{iso}/β interface. The O" phase exhibits a similar compositional behavior, but in contrast with the ω_{iso} phase, the Al content is higher, and only slightly less than that of Al in the matrix β phase, which reduces the Ti concentration, and this is qualitatively supported by the dark contrast of O" phase particles shown in the Z-contrast STEM images in Fig. 4(a) and 4(d). Here the composition of the O" phase is reported for the first time, and combined with our previous characterization of its crystal structure, provides a novel insight into its formation mechanism, i.e., where solute diffusion plays a critical role in the formation of nano-scaled ordered O" phase. Significant amounts of V, Mo and Cr, together with some Al, partition to the β phase from the incipient nano-scaled domains, generating the heating-induced ordered orthorhombic structure of the O" phase, mainly composed of Ti and approximately 7.6 at% Al – which, as well known, has a strong influence on the short range ordering in titanium alloys. Therefore, such nano-scaled partitioning of Al (compared with that in the nano-scaled ω_{iso} phase) assists in forming the ordered O" phase, rather than the long-ranged α" martensite.

In this work, two types of nano-scaled disordered and ordered phases with orthorhombic structures, namely the O' phase and O" phase, were characterized in the same metastable β-titanium alloy, Ti-5553. During quenching from above the β transus temperature, athermal ω phase and O' phase are formed in the parent β matrix by different atom shuffle mechanisms, exhibiting similar nanometer size scale particles, randomly distributed in the parent β phase. O' phase is stable in a wide range of temperatures up to the O' phase solvus temperature, which was measured to be between 200°C and 250°C for Ti-5553. Unlike the ω phase, no growth of O' phase or O' to α" transformation has been observed during aging yet, which is the reason that a shape memory effect has not been found in Ti-5553. Instead, a heating-induced ordered orthorhombic structure O" phase has been observed to form directly from β phase by slight partitioning of Al (compared with ω_{iso} phase, but still leaner than the β matrix) in the nano-scaled region resulting in the ordering of every third $\{011\}_{\beta}$ atom planes, rather than the heating-induced α" martensite in Ref. [25]. The formation of such O" phase occurs at temperatures higher than the O' phase solvus temperature, indicating there is no transition from shuffle-induced modulated structure to the heating-induced ordered structure.

Acknowledgement
This research has been supported by the National Science Foundation, Division of Materials Research, grant # DMR-1309270, DMREF grant DMR-1435483 and DMR-1905835. SA would

like to acknowledge the funding from the Natural National Science Foundation of China [grant No. 51850410518] and the China Postdoctoral Science Foundation [grant No. 2018M630069].

References:

[1] M. Abdel-Hady, K. Hinoshita, M. Morinaga, Scr. Mater., 55 (2006) 477-480.
[2] D. Kuroda, M. Niinomi, M. Morinaga, Y. Kato, T. Yashiro, Mater. Sci. Eng. A, 243 (1998) 244-249.
[3] A. Devaraj, S. Nag, R. Srinivasan, R.E.A. Williams, S. Banerjee, R. Banerjee, H.L. Fraser, Acta Mater., 60 (2012) 596-609.
[4] H.L. Wang, Y.L. Hao, S.Y. He, T. Li, J.M. Cairney, Y.D. Wang, Y. Wang, E.G. Obbard, F. Prima, K. Du, S.J. Li, R. Yang, Acta Mater., 135 (2017) 330-339.
[5] Y. Zheng, R.E.A. Williams, S. Nag, R. Banerjee, H.L. Fraser, D. Banerjee, Scr. Mater., 116 (2016) 49-52.
[6] M. Tahara, H.Y. Kim, T. Inamura, H. Hosoda, S. Miyazaki, Acta Mater., 59 (2011) 6208-6218.
[7] H. Tobe, H.Y. Kim, T. Inamura, H. Hosoda, S. Miyazaki, Acta Mater., 64 (2014).
[8] S.A. Mantri, D. Choudhuri, T. Alam, V. Ageh, F. Sun, F. Prima, R. Banerjee, Scr. Mater., 130 (2017) 69-73.
[9] J. Zhang, C.C. Tasan, M.J. Lai, A.C. Dippel, D. Raabe, Nat. Commun., 8 (2017) 14210.
[10] M.J. Lai, T. Li, D. Raabe, Acta Mater., 151 (2018) 67-77.
[11] E. Pang, E. Pickering, S.-I. Baik, D.N. Seidman, N.G. Jones, Acta Mater., 153 (2018) 62-70.
[12] M. Li, X. Min, K. Yao, F. Ye, Acta Mater., 164 (2019) 322-333.
[13] D. Banerjee, J.C. Williams, Acta Mater., 61 (2013) 844-879.
[14] J.D. Cotton, R.D. Briggs, R.R. Boyer, S. Tamirisakandala, P. Russo, N. Shchetnikov, J.C. Fanning, JOM, 67 (2015) 1281-1303.
[15] Y. Zheng, R.E.A. Williams, D. Wang, R. Shi, S. Nag, P. Kami, J.M. Sosa, R. Banerjee, Y. Wang, H.L. Fraser, Acta Mater., 103 (2016) 850-858.
[16] T. Li, J.M. Cairney, D. Kent, M.S. Dargusch, D. Kent, G. Sha, Scr. Mater., 104 (2015) 75-78.
[17] A. Devaraj, V.V. Joshi, A. Srivastava, S. Manandhar, V. Moxson, V.A. Duz, C. Lavender, Nat. Commun., 7 (2016) 11176.
[18] S.A. Mantri, D. Choudhuri, A. Behra, J.D. Coton, N. Kumar, R. Banerjee, Metall. Mater. Trans. A, 46 (2015) 2803-2808.
[19] M.J. Lai, C.C. Tasan, D. Raabe, Acta Mater., 100 (2015) 290-300.
[20] M.J. Lai, C.C. Tasan, J. Zhang, B. Grabowski, L.F. Huang, D. Raabe, Acta Mater., 92 (2015) 55-63.
[21] M.J. Lai, C.C. Tasan, D. Raabe, Acta Mater., 111 (2016) 173-186.
[22] Y. Yang, G.P. Li, G.M. Cheng, H. Wang, M. Zhang, F. Xu, K. Yang, Scr. Mater., 58 (2008) 9-12.
[23] Y. Yang, S.Q. Wu, G.P. Li, Y.L. Li, Y.F. Lu, K. Yang, P. Ge, Acta Mater., 58 (2010) 2778-2787.
[24] Y. Yang, P. Castany, E. Bertrand, M. Cornen, J.X. Lin, T. Gloriant, Acta Mater., 149 (2018) 97-107.
[25] J. Gao, Y. Huang, D. Guan, A.J. Knowles, L. Ma, D. Dye, W.M. Rainforth, Acta Mater., 152 (2018) 301-314.
[26] P. Castany, Y. Yang, E. Bertrand, T. Gloriant, Phys. Rev. Lett., 117 (2016).

[27] M. Tahara, T. Kanaya, H.Y. Kim, T. Inamura, H. Hosoda, S. Miyazaki, Acta Mater., 80 (2014) 317-326.
[28] H.Y. Kim, L. Wei, S. Kobayashi, M. Tahara, S. Miyazaki, Acta Mater., 61 (2013) 4874-4886.
[29] Y. Zheng, D. Huber, H.L. Fraser, Scr. Mater., 154 (2018) 220-224.
[30] A.J. Knowles, N.G. Jones, O.M.D.M. MessÈ, J.S. Barnard, C.N. Jones, H.J. Stone, Int. J. Refract. Metals. Hard. Mater., 60 (2016) 160-168.
[31] A.J. Knowles, T.-S. Jun, A. Bhowmik, N.G. Jones, T.B. Britton, F. Giuliani, H.J. Stone, D. Dye, Scr. Mater., 140 (2017) 71-75.
[32] G.I. Nosova, N.B. Dyakonova, I.V. Lyasotskii, Met. Sci. Heat. Treat., 48 (2006) 427-432.
[33] Y. Zheng, D. Banerjee, H.L. Fraser, Scr. Mater., 116 (2016) 131-134.
[34] Y. Zheng, T. Alam, R. Banerjee, D. Banerjee, H.L. Fraser, Scr. Mater., 152 (2018) 150-153.
[35] Y. Wang, J. Gao, H. Wu, S. Yang, X. Ding, D. Wang, X. Ren, Y. Wang, X. Song, J. Gao, Sci. Rep., 4 (2014).
[36] Y. Zheng, R.E.A. Williams, H.L. Fraser, Scr. Mater., 113 (2016) 202-205.
[37] M.B. Bettaieb, A. Lenain, A.M. Habraken, Fatigue. Fract. Eng. M., 36 (2013) 401-415.
[38] S. Sadeghpour, S.M. Abbasi, M. Morakabati, A. Kisko, L.P. Karjalainen, D.A. Porter, Scr. Mater., 145 (2018) 104-108.
[39] J. Coakley, A. Radecka, D. Dye, P.A.J. Bagot, T.L. Martin, T.J. Prosa, Y. Chen, H.J. Stone, D.N. Seidman, D. Isheim, Mater. Charact., 141 (2018) 129-138.
[40] T. Li, D. Kent, G. Sha, H. Liu, S.G. Fries, A.V. Ceguerra, M.S. Dargusch, J.M. Cairney, Scr. Mater., 155 (2018) 149-154.

Figure Caption:

Figure 1. TEM and S/TEM characterization of O′ phase in the as-quenched state Ti-5553: (a) $[011]_\beta$ zone axis pattern and (b) corresponding dark field image selecting reflection highlighted in (a) showing the co-existence of athermal ω phase and O' phase; (c) $[100]_\beta$ zone axis pattern and (d) corresponding dark field image selecting O′ reflection highlighted in (b) showing O' phase; (e) HAADF-STEM image showing the shuffle induced O′ phase of orthorhombic structure.

Figure 2. TEM diffraction patterns recorded from $[100]_\beta$ zone axis using in-situ heating holder at elevated temperatures showing the stability of the O′ phase, with intensity profile along yellow dotted line as inset: (a) 20°C; (b) 50°C; (c) 100°C; (d) 150°C; (e) 200°C; (f) 250°C; (g) 300°C; (h) 350°C

Figure 3. TEM diffraction patterns and dark field images showing the microstructure of Ti-5553 aged to 350°C (a-c) and 375°C (d-f) respectively: (a) $[011]_\beta$ zone axis diffraction; (b) $[100]_\beta$ zone axis diffraction pattern: (c) corresponding dark field image selecting reflections highlighted in (a) showing the presence of isothermal ω phase and O' phase at 350°C; (d) $[011]_\beta$ zone axis diffraction; (e) $[100]_\beta$ zone axis diffraction pattern: (f) corresponding dark field image selecting reflections highlighted in (e) showing the presence of O" phase at 375°C

Figure 4. HAADF-STEM images showing the ordered orthorhombic structure of O" phase: (a) low magnification image showing the co-existence of two O" phase variants; (b-c) local FFT of two O" phase variants individually; (d) high magnification image showing the ordering in the

center of O" phase particle; (e) 3D reconstruction showing the Ti atoms, 85 at.% isconcentration surfaces (O" phase), and 6.5 at.% Al isconcentration surfaces (ω_{iso} phase); (f-g) an O" and ω_{iso} precipitate, respectively; (h-i) Ti and Al 2D concentration surfaces from a 10×10×5 nm thick slice of the precipitate in (f) and (g), respectively; (j-k) proxigrams with respect to the isoconcetration surfaces delineating the O" and ω_{iso} precipitates in (f) and (g), respectively.

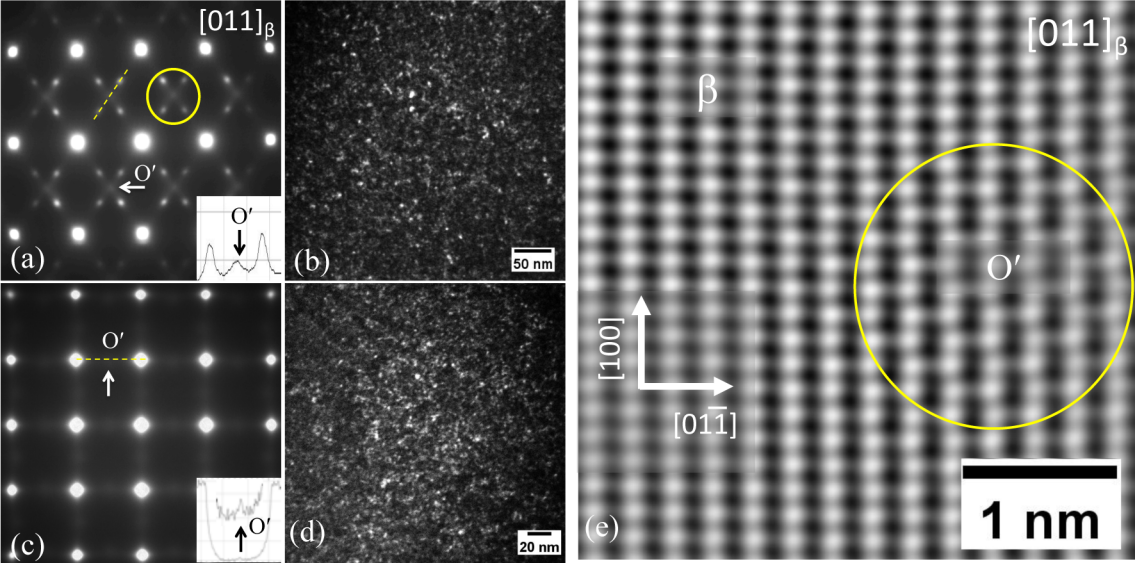
[011]β
O′
(a)
O′
(b)
50 nm
O′
(c)
O′
(d)
20 nm
[011]β
β
O′
[100]
[01$\bar{1}$]
(e)
1 nm

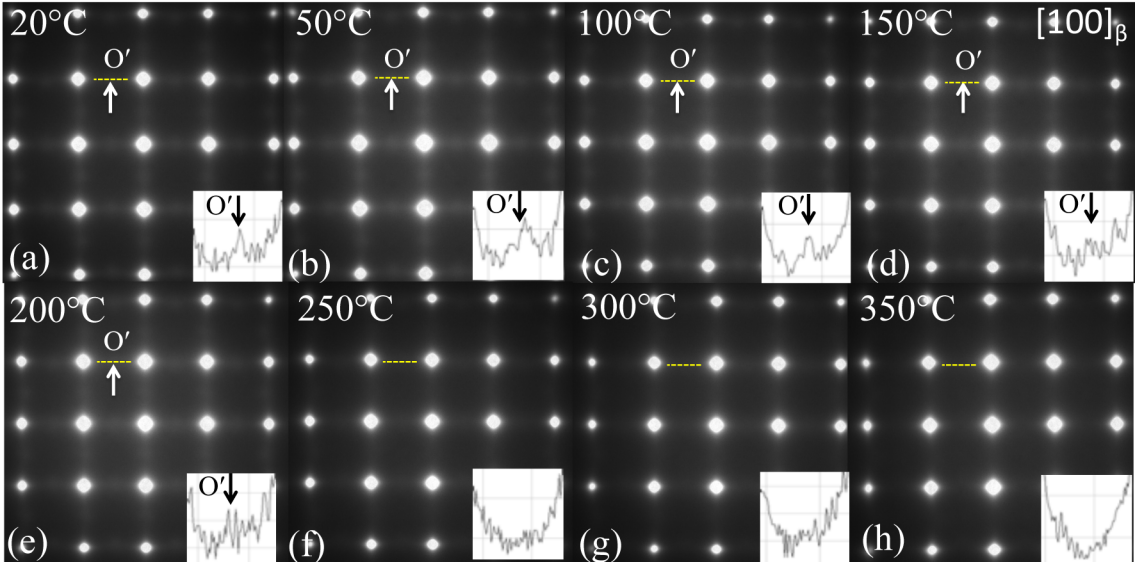
20°C
O′
(a)
50°C
O′
(b)
100°C
O′
(c)
150°C
O′
[100]β
(d)
200°C
O′
(e)
250°C
(f)
300°C
(g)
350°C
(h)

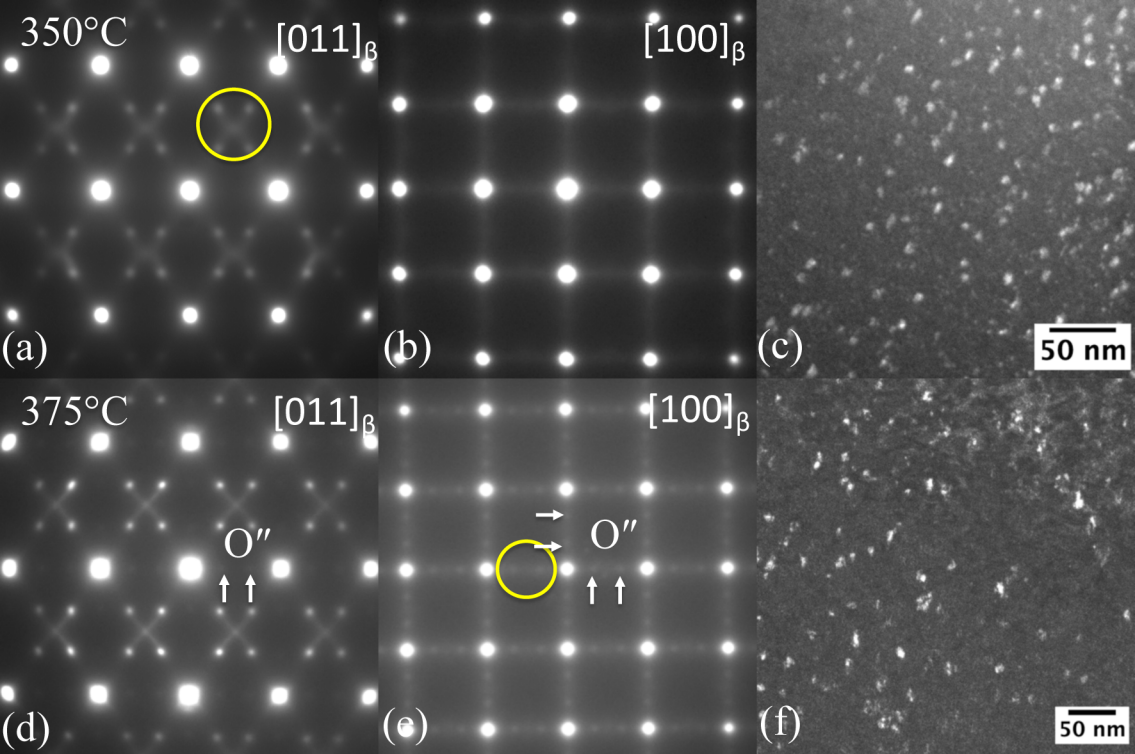
350°C
[011]β
[100]β
(a)
(b)
(c)
50 nm
375°C
[011]β
[100]β
O″
O″
(d)
(e)
(f)
50 nm

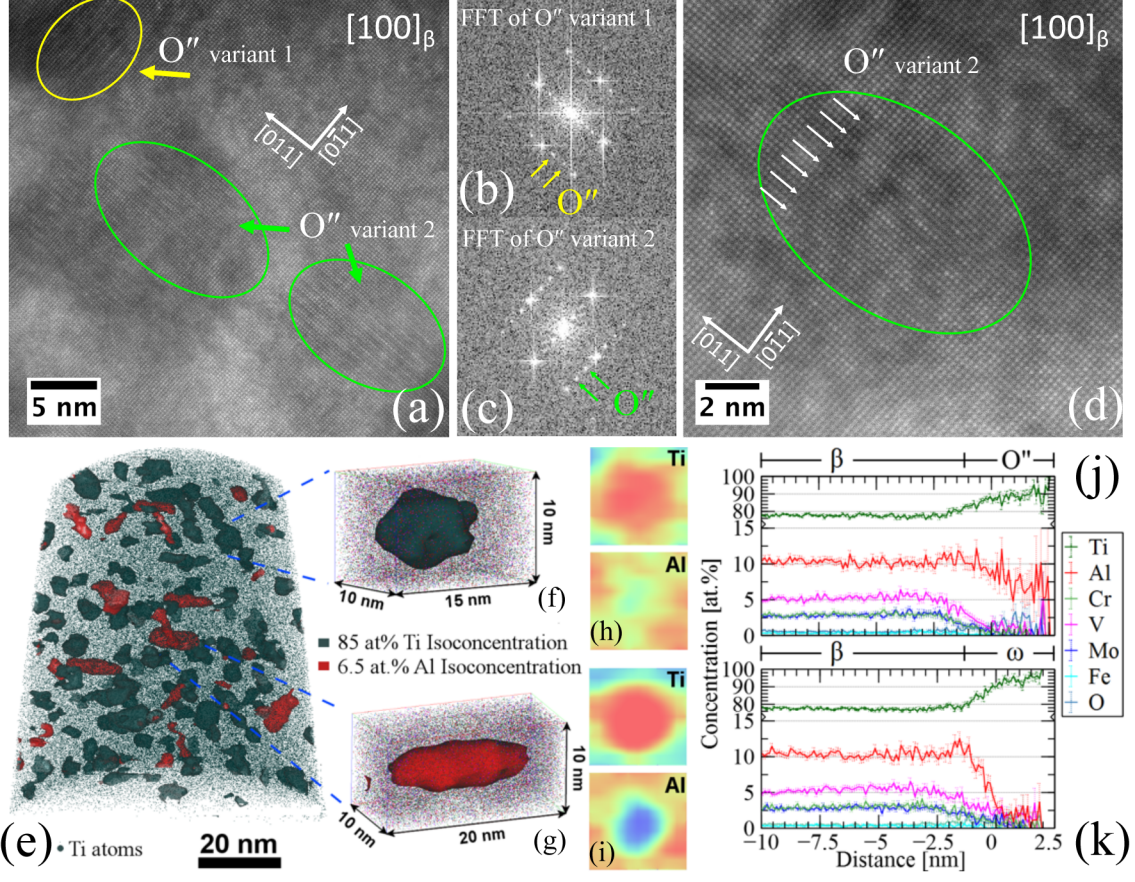
[100]β
O″ variant 1
[011]
[01̄1]
O″ variant 2
5 nm
(a)
FFT of O″ variant 1
(b)
O″
FFT of O″ variant 2
O″
(c)
[100]β
O″ variant 2
[011]
[01̄1]
2 nm
(d)
(e)
• Ti atoms
20 nm
10 nm
15 nm
(f)
10 nm
20 nm
(g)
85 at% Ti Isoconcentration
6.5 at.% Al Isoconcentration
Ti
Al
(h)
Ti
Al
(i)
β
O″
β
ω
Concentration [at.%]
Distance [nm]
Ti
Al
Cr
V
Mo
Fe
O
(j)
(k)

Table 1. Nominal composition of Ti5553, as measured by wet chemistry, along with atom probe tomography measured nominal, β phase, ω phase, and O" phase compositions.

Ion/Phase	Wet Chemistry Nominal [wt.% (at.%)]	Atom Probe Compositions [at.%]			
		Nominal	β	ω	O"
Ti	BALANCE	78.1 +/- 0.02	77.3 +/- 0.7	93.4 +/- 1.9	88.5 +/- 3.0
Al	5.67 (9.90)	10.4 +/- 0.01	10.3 +/- 0.5	1.93 +/- 1.0	7.6 +/- 1.9
Mo	5.00 (2.46)	2.6 +/- 0.01	2.8 +/- 0.3	0.4 +/- 0.6	0.4 +/- 0.6
V	4.92 (4.55)	4.9 +/- 0.01	5.4 +/- 0.4	1.7 +/- 0.9	1.2 +/- 1.2
Cr	3.04 (2.75)	2.9 +/- 0.01	3.0 +/- 0.3	0.6 +/- 0.6	0.4 +/- 0.5
Fe	0.48 (0.40)	0.3 +/- 0.00	0.4 +/- 0.1	0.1 +/- 0.2	0.1 +/- 0.1
O	0.18 (0.53)	0.6 +/- 0.00	0.5 +/- 0.1	1.4 +/- 0.8	1.8 +/- 1.3
Ga	N/A	0.01 +/- 0.01	0.01 +/-0.02	0.05 +/-0.01	0.00 +/- 0.00

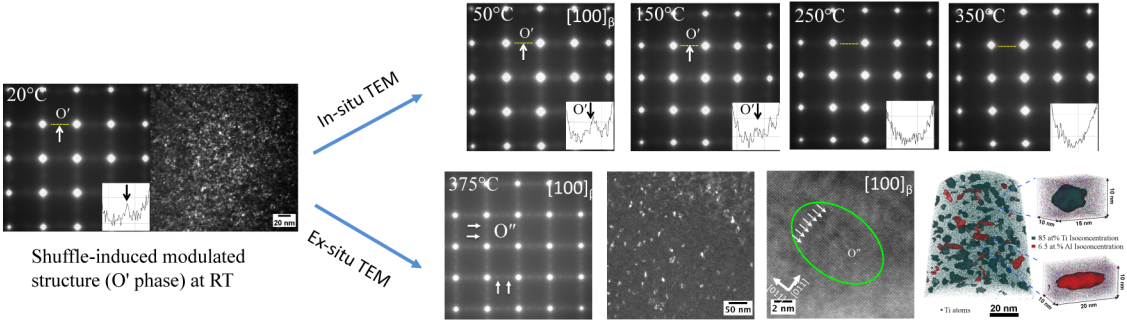
Shuffle-induced modulated structure stable from RT to elevated temperature
20°C
O′
20 nm
In-situ TEM
Ex-situ TEM
50°C
[100]β
O′
150°C
O′
250°C
350°C
375°C
[100]β
O″
50 nm
[100]β
O″
2 nm
[001]
[110]
• Ti atoms
20 nm
85 at% Ti Isoconcentration
6.5 at.% Al Isoconcentration
10 nm
15 nm
20 nm
Shuffle-induced modulated structure (O′ phase) at RT
Heating-induced ordered structure (O″ phase) at 375°C